

國立中央大學

機械工程研究所

碩/博士論文

模版 ncuthesisCJK 使用說明

An example in L<sup>A</sup>T<sub>E</sub>X/XeL<sup>A</sup>T<sub>E</sub>X

研究生: 羅吉昌

指導教授: 羅吉昌

共同指導: 甲教授  
乙教授

中華民國一百零二年六月



國立中央大學

機械工程研究所  
碩/博士論文

模版 ncuthesisCJK 使用說明  
An example in L<sup>A</sup>T<sub>E</sub>X/XeL<sup>A</sup>T<sub>E</sub>X

研究生: 羅吉昌

指導教授: 羅吉昌

共同指導: 甲教授  
乙教授

中華民國一百零二年六月

版權所有© 羅吉昌 2012





## 國立中央大學圖書館 碩博士論文電子檔授權書

(101 年 9 月最新修正版)

本授權書授權本人撰寫之碩/博士學位論文全文電子檔(不包含紙本、詳備註 1 說明)，在「國立中央大學圖書館博碩士論文系統」。(以下請擇一勾選)

- ( ☐ )**同意** (立即開放)  
( ☐ )**同意** (請於西元 \_\_\_\_\_年\_\_\_\_月\_\_\_\_日開放)  
( ☐ )**不同意**，原因是：\_\_\_\_\_

在國家圖書館「臺灣博碩士論文知識加值系統」

- ( ☐ )**同意** (立即開放)  
( ☐ )**同意** (請於西元 \_\_\_\_\_年\_\_\_\_月\_\_\_\_日開放)  
( ☐ )**不同意**，原因是：\_\_\_\_\_

以非專屬、無償授權國立中央大學、台灣聯合大學系統圖書館與國家圖書館，基於推動「資源共享、互惠合作」之理念，於回饋社會與學術研究之目的，得不限地域、時間與次數，以紙本、微縮、光碟及其它各種方法將上列論文收錄、重製、與利用，並得將數位化之上列論文與論文電子檔以上載網路方式，提供讀者基於個人非營利性質之線上檢索、閱覽、下載或列印。

研究生簽名：\_\_\_\_\_ 學號：\_\_\_\_\_

論文名稱：\_\_\_\_\_

指導教授姓名：\_\_\_\_\_

系所：\_\_\_\_\_所 ☐博士班 ☐碩士班

備註：

1. 本授權書之授權範圍僅限電子檔，紙本論文部分依著作權法第 15 條第 3 款之規定，採推定原則即預設同意圖書館得公開上架閱覽，如您有申請專利或投稿等考量，不同意紙本上架陳列，須另行加填聲明書，詳細說明與紙本聲明書請至 <http://thesis.lib.ncu.edu.tw/> 下載。
2. 本授權書請填寫並**親筆**簽名後，裝訂於各紙本論文封面後之次頁（全文電子檔內之授權書簽名，可用電腦打字代替）。
3. 請加印一份單張之授權書，填寫並親筆簽名後，於辦理離校時交圖書館（以統一代轉寄給國家圖書館）。
4. 讀者基於個人非營利性質之線上檢索、閱覽、下載或列印上列論文，應遵守著作權法規定。





國立中央大學碩士班研究生  
論文指導教授推薦書

\_\_\_\_\_學系/研究所\_\_\_\_\_研究生所提之論文  
\_\_\_\_\_ 係由本  
( 題 目 )

人指導撰述，同意提付審查。

指導教授\_\_\_\_\_ (簽章)

\_\_\_\_年\_\_\_\_月\_\_\_\_日







國立中央大學博士班研究生

## 論文口試委員審定書

\_\_\_\_\_學系/研究所\_\_\_\_\_研究生所提之論文

\_\_\_\_\_

經本委員會審議，認定符合博士資格標準。

學位考試委員會召集人 \_\_\_\_\_  
委 員 \_\_\_\_\_  
\_\_\_\_\_  
\_\_\_\_\_  
\_\_\_\_\_

中 華 民 國                      年                      月                      日





模版 ncuthesisCJK 使用說明

An example in L<sup>A</sup>T<sub>E</sub>X/XeL<sup>A</sup>T<sub>E</sub>X

### 中文摘要

關鍵字：碩博士論文，體裁檔，L<sup>A</sup>T<sub>E</sub>X，XeL<sup>A</sup>T<sub>E</sub>X

此論文範例得以完成是由於體裁檔(ncuthesis.cls)的完成。期間多方閱讀、吸收、漸有所獲，直至發掘兩篇網路文章，深入了解後再加入中文化及適當增修而成。本體裁檔可再增修，複製，直接採用做個人用途，或供單位使用，唯不可做商業用途。

此套件係自助編寫屬非賣品，可自由使用，但不做任何保證。期望提供學生便利性，做出符合國立中央大學所規範的研究所論文格式，但不隱含任何商業價值。[Open NCU Thesis Requirements](https://code.google.com/p/ncu-thesis-latex-template/)

### 來源

<https://code.google.com/p/ncu-thesis-latex-template/>

### 功能

- 論文格式滿足本校要求。
- Unicode/UTF8 中文化。
- 可選擇編譯方式(pdfL<sup>A</sup>T<sub>E</sub>X，XeL<sup>A</sup>T<sub>E</sub>X)。
- 可選單面印刷或雙面印刷。
- 快速編譯及越界偵錯。
- 可列印紙張結構及參數。
- 顯示智財權及製作日期。
- 具索引及浮水印功能。
- 其它文書製作及提醒功能。
- 如何使用體裁檔請看第一章說明。
- 如何使用L<sup>A</sup>T<sub>E</sub>X 請看第二章說明。
- 如何製作參考文獻請看第三章說明。





模版 ncuthesisCJK 使用說明

An example in  $\text{\LaTeX}$ / $\text{Xe}\text{\LaTeX}$

### 英文摘要

Keywords: Master/Doctorial thesis, Class file,  $\text{\LaTeX}$ ,  $\text{Xe}\text{\LaTeX}$

The files included in the directory are free to use, copy, or modify for personal use or within an organization. Primarily, the files are for graduates who want to write their theses in  $\text{\LaTeX}$ / $\text{Xe}\text{\LaTeX}$  and meet the requirements stipulated by the National Central University.

This document is distributed in the hope that it will be useful to graduates, but without any warranty; without even the implied warranty of merchantability.

### Source

<https://code.google.com/p/ncu-thesis-latex-template/>

### Features

- Master/Doctorial thesis stipulated by National Central University.
- Unicode/UTF8 supports.
- Compilable by  $\text{pdf}\text{\LaTeX}$  or  $\text{Xe}\text{\LaTeX}$ .
- Oneside or twoside printing.
- Fast compilation and overfull detection.
- Page layout and parameters.
- Copyright and time stamp.
- Index, watermark capabilities.
- Other thesis variants and todonote reminder.
- How to use this package — Chapter 1.
- How to use  $\text{\LaTeX}$  (very brief) — Chapter 2.
- How to generate references — Chapter 3.





模版 ncuthesisCJK 使用說明

An example in L<sup>A</sup>T<sub>E</sub>X/XeL<sup>A</sup>T<sub>E</sub>X

### 謝誌

體裁檔受啓發於兩位英美教授於網路上的文章，並經吾人中文化及適當增修而成。本體裁檔可再增修，複製，直接採用做個人用途，或單位使用，唯不可做商業用途。請尊重上述兩位教授的無私奉獻。

- 感謝T<sub>E</sub>X/L<sup>A</sup>T<sub>E</sub>X網路社群內，龐大的T<sub>E</sub>X/L<sup>A</sup>T<sub>E</sub>X社群及其網頁提供無價資訊。
- 欣逢中央大學教務處註冊組組長，蕭嘉璋老師，見微知著，並予協助，僅此誌謝。
- 承蒙太空及遙測研究中心蔡富安老師協助在Ubuntu 12.04上TeXLive-2009測試成功，僅此誌謝。
- 2013/06/13碩士班 葉信麟同學發現目錄頁碼不正確。
- 2013/07/04碩士班 林億同學發現附錄節碼不正確。







# Contents

	頁次
中文摘要 .....	i
英文摘要 .....	iii
謝誌 .....	v
目錄 .....	vii
圖目錄 .....	ix
表目錄 .....	xi
符號說明 .....	xv
1. Introduction .....	1
2. Methods .....	5
2.1 Laboratory Astrophysics . . . . .	5
2.1.1 Experimental simulations by IPS system . . . . .	5
2.1.2 Vacuum-UV source . . . . .	8
2.1.3 Extreme EUV source . . . . .	9
2.2 Experimental Protocol . . . . .	10
2.3 Infra-red spectroscopy and the Beer's Law . . . . .	11
2.4 Reaction Rate Laws . . . . .	13
3. Experimental Results of $\text{CH}_4 + \text{NH}_3$ ice mixtures .....	17
3.1 3.1.1 The concentration effect of $\text{CH}_4$ on production of $\text{C}_2\text{H}_6$ and $\text{CN}^-$ . . . . .	18
3.2 3.1.1 Reaction mechanisms . . . . .	20
索引 .....	21
參考文獻 .....	21





## List of Figures

圖 2.1	The schematic diagram of IPS system, mechanical pumps are not shown for clarity. (Quoted from Chen et al. 2014)	6
圖 2.2	The cross-section of MDHL (T-type geometry) (Quoted from Chen et al. 2014).	8
圖 2.3	VUV spectra of MDHL (T-type geometry, 110-180 nm) with different H <sub>2</sub> pressure inside the lamp(Quoted from Chen et al. 2014).	9
圖 2.4	Different vibrational modes of a three atom molecule.	12





## List of Tables

表 3.1	The peak positions of identified substances after irradiation in different configurations of ice mixtures. . . . .	19
表 3.2	The strength of absorbance adopted in this thesis measured in literatures of pure ice samples . . . . .	20





# Todo list

完稿時要用[disable]除去所有todos。 . . . . . xiii

完稿時要用[disable]除去所有todos。







## 模版 ncuthesisCJK 使用說明

An example in L<sup>A</sup>T<sub>E</sub>X/XeL<sup>A</sup>T<sub>E</sub>X

### 符號說明

<code>\dept</code>	: 研究所
<code>\degree</code>	: 碩/博士 or 專題研究 or 論文計畫書
<code>\title</code>	: 論文中文題目
<code>\subtitle</code>	: 論文英文題目
<code>\logo</code>	: 封面校徽(預設中央校徽)
<code>\author</code>	: 作者
<code>\mprof</code>	: 指導教授
<code>\sprof</code> , <code>\sprofii</code>	: 兩位共同指導
<code>\degreedate</code>	: 中華民國 XXX 年 X 月
<code>\copyyear</code>	: 著作完成年
<code>\includepdf</code>	: 插頁指令，需pdfpages巨集
<code>\fontsize...</code> <code>\selectfont</code>	: 設定字大小行距
<code>\bookbone</code>	: 書脊短時用
<code>abstractcn</code>	: 中文摘要環境名，檔案則為abstractcn.tex
<code>abstracten</code>	: 中文摘要環境名，檔案則為abstracten.tex
<code>acknowledgements</code>	: 謝誌環境名，檔案則為acknowledge.tex
<code>appendA</code>	: 附錄一環境名，檔案則為appendix.tex
<code>appendB</code>	: 附錄二環境名，檔案則為appendix.tex
<code>symbols</code>	: 符號說明環境名，檔案則為symbol.tex





# 1. Introduction

According to Hindu cosmological mythology, ancient people believe that a giant turtle bears the world on its back. Even after we stepped onto the moon at 1969, there are still plenty that we cannot explain. In the novel *Lord of the Rings*, the author named the path between hobbits as Mordor, which is also the name of the dark area on Pluto's moon, Charon. Recently, Mission New Horizons retrieved valuable data about Charon and Pluto. This thesis aims to explain the formation mechanisms of the red cap on the pole of Charon (fig. 1), especially during the long cold dark period, through observations in extreme ultra-violet (EUV) and vacuum ultra-violet (VUV) irradiation.

## Composition of Charon

The main composition on the surface of Charon is  $\text{H}_2\text{O}$ . According to Infrared (IR) spectroscopy, it is a mixture of 90 %  $\text{H}_2\text{O}$  and 10 % tholin at millimetre depth. The second most dominant component is ammonia hydrate, which can be observed by earth-based telescopes (brown 2000, cook 2007). In far IR spectrum taken by LEISA camera on the New Horizons, concentrated ammonia is found on Organa crater (fig 2.) and throughout Charon (fig 3.) (Grundy 2016a). The third component which forms the dark red cap (tholin?) is cold-trapped methane from Pluto's atmosphere ejecta (Hoey 2017). The presence of nitrogen and other ejecta from Pluto are neglected in this thesis because according to the model of Hoey et al. (2017) (fig.4), during New horizons' approach, 98 % of the arrived ejecta is  $\text{CH}_4$ . Charon's atmospheric pressure is further constrained by New Horizons to be below 0.3 nano bars, which is  $4 \times 10^{-13}$  torr for all 14 atoms and molecules including  $\text{CO}$ ,  $\text{H}_2$ ,  $\text{CH}_4$ ,  $\text{Ne}$ ,  $\text{Ar}$ , etc. (fig. 5).  $\text{CH}_4$  remains undetectable when we convert the momentum of  $\text{CH}_4$  with 7 hops on the surface of Charon until deposited onto cold enough part is  $1 \times 10^{-11}$  Pa, which is  $7.5 \times 10^{-14}$  torr (Grundy



2016b).

#### VUV irradiation

Ly- $\alpha$  appears to be the largest source in the dark side of Charon, with attributions from both solar occultation (70 %) and resonance scattering by atomic hydrogen flow (30 %) in the solar system at flux  $3.5 \times 10^7$  photons  $\text{cm}^{-2} \text{s}^{-1}$  onto the winter pole of Charon (Grundy 2016b). The flux is 50 % larger than expected before Mission New Horizons (Gladstone 2015).  $\text{CH}_4$  deposits at temperature below 25 K at pressure  $7.4 \times 10^{-14}$  torr. The time for depositing  $\text{CH}_4$  is 2 times longer at the pole (130 earth years) than at 45 latitude according to the thermal model of Grundy et al. (2016b) (fig 6). In order to understand the formation of tholin at different latitudes of Charon, we performed VUV irradiation on  $\text{CH}_4 + \text{NH}_3$  and  $\text{CH}_4 + \text{NH}_3 + \text{H}_2\text{O}$  experiments with different ratios (including 3:2, 1:5, 1:10 and 1:20 for  $\text{CH}_4 + \text{NH}_3$  and 5:3:4, 1:5:5 and 1:10:10 for  $\text{CH}_4 + \text{NH}_3 + \text{H}_2\text{O}$  ice mixtures) to simulate the conditions at different latitudes on Charon with base pressure  $3 \times 10^{-10}$  torr, simulating atmosphere on Charon at 15 K, which corresponds to temperature on Charon at winter times (Grundy 2016b) in interstellar processing system (IPS) (Chen 2014).

#### EUV irradiation

Apart from VUV irradiation, EUV irradiation also took part. VUV irradiation is believed to be the main process to convert  $\text{CH}_4$  into heavier molecules which remained on the surface of Charon until the temperature of Charon become 60 K, at which methane evaporates from the ice. The ice is then further processed by EUV, solar wind, coronal mass ejections and interstellar pickup ions, etc to produce the tholin on Charon (Grundy 2016b). The EUV irradiation ( $>12.4$  eV) is  $8.7 \times 10^7 \text{ eV cm}^{-2} \text{s}^{-1}$  at mean heliocentric distance 39 A.U. whereas VUV irradiation (Ly- $\alpha$ ) is  $1.9 \times 10^9 \text{ eV cm}^{-2} \text{s}^{-1}$ . In order to investigate the effectiveness of EUV to VUV irradiation, we kept temperature of  $\text{CH}_4 + \text{NH}_3$  (3:2 & 1:5) and  $\text{CH}_4 + \text{NH}_3 + \text{H}_2\text{O}$  (5:3:4) ice mixtures at 15 K and use the monochromatic 30.4 nm (He II) light provided by High flux beamline at National Synchrotron Radiation Research Centre (NSRRC) in Taiwan to irradiate the ice mixtures.



H<sub>2</sub>O involved?

We compared the conditions of CH<sub>4</sub>+NH<sub>3</sub> and CH<sub>4</sub>+NH<sub>3</sub>+H<sub>2</sub>O because tholin on Titan is believed to be formed by CH<sub>4</sub>+N<sub>2</sub> and a similar colour was observed on Charon. Charon is different from Titan as H<sub>2</sub>O dominates on Charon. What are the differences between tholin formed by CH<sub>4</sub>+NH<sub>3</sub> and CH<sub>4</sub>+N<sub>2</sub>? What role does H<sub>2</sub>O play on Charon in the formation of tholin? Is it just diluting the formation or new compounds are formed?

In this thesis, we will introduce the formation reaction mechanisms of CH<sub>4</sub>+NH<sub>3</sub> ice mixtures in EUV and VUV irradiation (section 3), the formation reaction mechanisms of CH<sub>4</sub>+NH<sub>3</sub>+H<sub>2</sub>O ice mixtures in EUV and VUV irradiation (section 4), and the residues of these mixtures and a brief comparison with tholin on Titan will be made (section 5). With these results, we will have a better understanding about Charon and some astrophysical implications will be presented (section 6).





## 2. Methods

### 2.1 Laboratory Astrophysics

To study the chemical reactivity in astrophysical environment experimentally, we conducted our experiments in Interstellar photoprocessing system (IPS) (Chen et al. 2014), an ultrahigh vacuum chamber with base pressure  $3 \times 10^{-10}$  torr and 14 K, corresponds to a density of  $10^6 \text{ cm}^{-3}$ , similar to dense cloud interiors. The system will be introduced in detail in section 2.1.1. To simulate the irradiation in interstellar environments, we use a micro-wave discharge hydrogen lamp (MDHL) and monochromatic extreme-ultraviolet irradiation (EUV) 30.4 nm to irradiate our ice mixtures, and they will be introduced in section 2.1.2 and 2.1.3 respectively. The experimental protocols will be elaborated in section 2.2. In order to better understand the physics behind, some basic theories of Infrared spectroscopy and concepts of chemical kinetics used in data analysis are included in section 2.3 and 2.4 respectively. To demonstrate the ice mixtures in KBOs, we used different configurations of ice mixtures that refers to different sections in chapter 3 and chapter 4.

#### 2.1.1 Experimental simulations by IPS system

We conducted our astrophysical simulations studied in chapter 3 to 4 in Interstellar Photo Processing System (IPS) (figure 2.1). IPS consists in three systems: the main chamber, where our experiments take places; the detection system, where we collect our data; and a gasline system, where we prepare our samples.

The main system consists of an ultrahigh vacuum chamber equipped with a closed-cycle helium cryostat (CTI-M350). It is pumped by a turbo molecular pump (KTKT FF – 160/620ZE, capacity  $600 \text{ liters s}^{-1}$ ), which is backed up by a scroll pump, and a non –evaporation get-

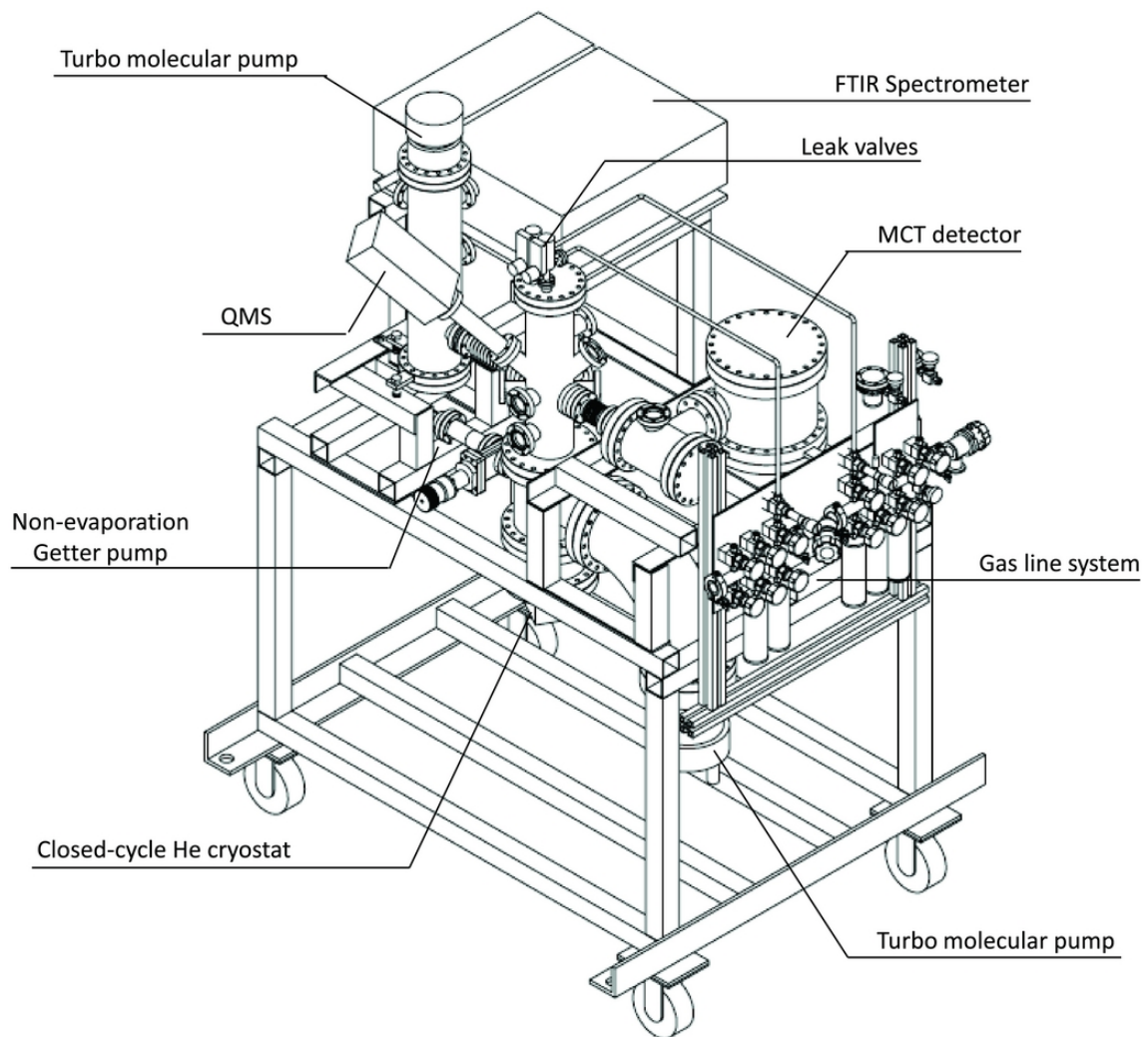


Figure 2.1: The schematic diagram of IPS system, mechanical pumps are not shown for clarity. (Quoted from Chen et al. 2014)





ter pump. The getter pump is a powerful tool to adsorb residue gases inside the main chamber, with a larger surface area,  $\text{H}_2$ ,  $\text{CO}$  and  $\text{N}_2$  are adsorbed to obtain a better base pressure. After baking, the base pressure of our main chamber can reach  $1 \times 10^{-10}$  torr at 14 K, monitored by a Granville-Phillips 370 Stabil-Ion gauge. This pressure can be used to demonstrate the dense cloud interior environments and star forming region. The substrate we have chosen is KBr, which can allow infra-red photons with 700 to 4000  $\text{cm}^{-1}$  to penetrate. It is mounted by substrate holder made of oxygen-free copper, on the first stage of cold finger mounted on the tip of cryostat. Two silicon diodes and also a heater were placed onto the cold finger and one of the silicon diodes is near the substrate holder. They were connected to a temperature controller and PID system to achieve a warmup rate of 1K/min with an accuracy of 0.1 K.

The detection system consists in a mid-infrared Fourier transform spectrometer (mid-FTIR) (ABB FTLA2000-104) and a Quadrupole Mass Spectrometer (QMS). To prevent absorption bands of  $\text{CO}$ ,  $\text{CO}_2$  and  $\text{H}_2\text{O}$  gas in the atmosphere, the IR beam path was built inside vacuum, pumped by dry pump. The main chamber and the IR path are separated by ZnSe windows, which can allow infra-red penetration from 0.5 – 20  $\mu\text{m}$  with absorption less than 0.07 %. In this study, the infrared spectra are obtained with resolution of 4  $\text{cm}^{-1}$  and averaged over 32 scans. The angle between the IR beam path and the substrate holder is 45 degrees. The QMS (MKS Microvision 2) consists of a controller and mechanical part sealed by a mounting flange in ultrahigh vacuum. It is mounted 10 cm from the substrate and run with a resolution 0.5 a.m.u. The Ionizer release 70 eV electron by filament and ionize incoming molecules to positive charged ions between anode grid and repeller. The ions were accelerated by focus plate and enters ion filter, which consists of four circular rods, with a combination of A.C and D.C. potential to sieve whole bandpass ions at millisecond timescale. The selected ions enter ion detector and are detected by either faraday cup and continuous dynode electron multiplier (CDEM) which can secondary multiply weak signals.

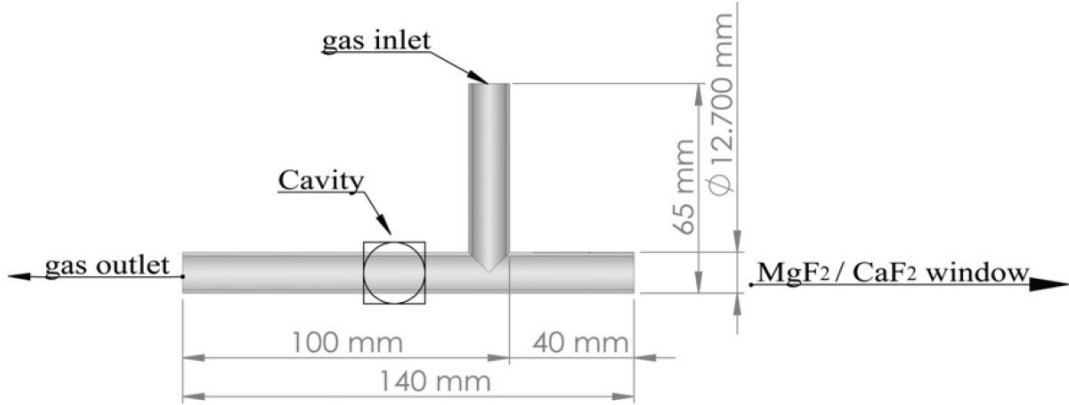


Figure 2.2: The cross-section of MDHL (T-type geometry) (Quoted from Chen et al. 2014).

The samples are prepared in situ in our gasline system. It contains four stainless steel bottles with the same volume, which is used to determine relative proportion of the gas mixtures by their partial pressures. The ammonia gas 99.99 % and methane 99.999 % are mixed with partial pressure measured by a Baratron with 0 - 100 torr range with a 0.25

### 2.1.2 Vacuum-UV source

In order to simulate the photoprocessing of vacuum ultraviolet (VUV) irradiation onto the interstellar ices and ices on planetary bodies, including KBOs, the ice mixtures are irradiated with a T-type Microwave-Discharged Hydrogen-flow lamp (MDHL). The molecular hydrogen with pressure 0.4 torr flows through the lamp with a support of a mechanical pump. Using a 2.4 GHz microwave generator and high voltage discharge, a low pressure plasma is produced in the Evenson cavity. Figure 2.2 shows a cross-section of T-type quartz tube; the middle part of the T-type quartz tube is being tunned by a ceramic rod that is called Evenson cavity. In order to measure the photon flux in situ, we use an 88 % transmittance nickel mesh with its photoelectric efficiency being obtained by high-flux beamline in National Synchrotron and a SXUV 100 photodiode calibrated by NIST. A  $\text{MgF}_2$  window is placed between the lamp and the sample holder to prevent penetration of VUV photons with wavelength shorter than 114nm, leads to a cut off at 114nm. Figure 2.3 shows a VUV emission spectrum of a MDHL. It consists in  $\text{Ly-}\alpha$  (121.6nm) and  $\text{H}_2$  molecular emission in 110-180 nm

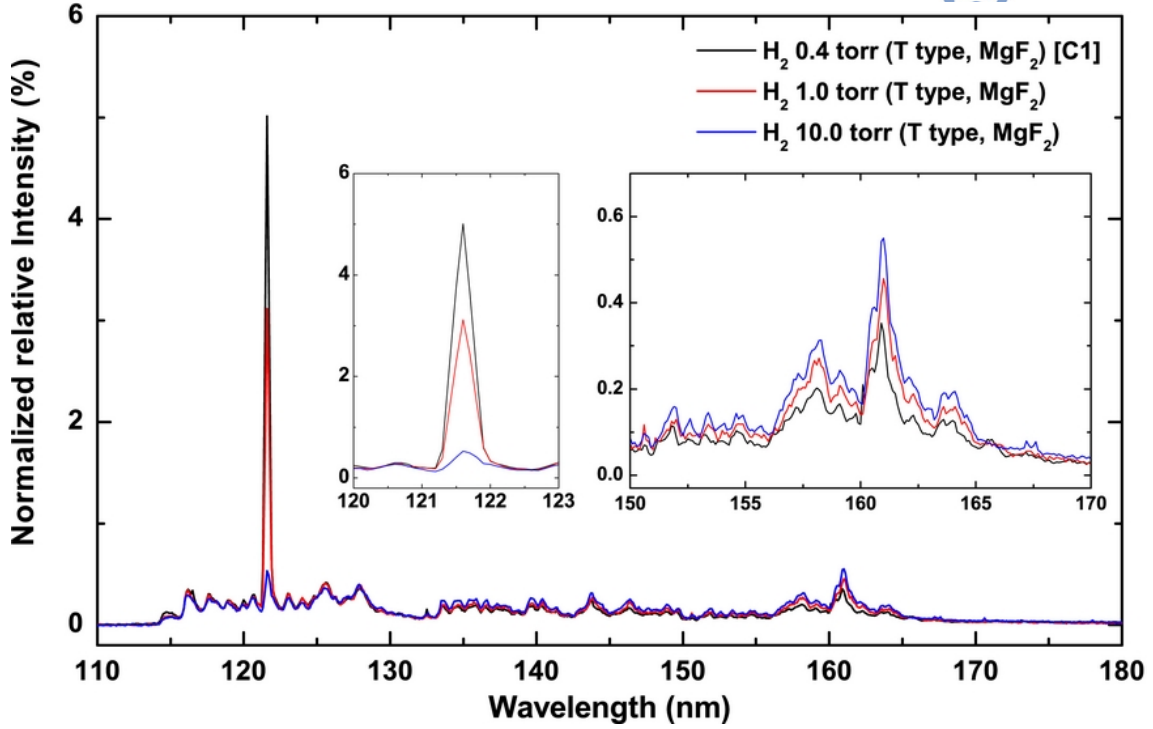


Figure 2.3: VUV spectra of MDHL (T-type geometry, 110-180 nm) with different  $H_2$  pressure inside the lamp (Quoted from Chen et al. 2014).

range. Chen et al. (2014) showed that the spectral characteristics of the VUV light emitted in this range depends on the gas type (mixture of  $H_2$  with He or Ar etc), pressure of  $H_2$  and lamp geometry. Throughout those configurations stated there, we adopted 0.4 torr molecular hydrogen and T-type MDHL that produces VUV irradiation at 114-170 nm with 19.1 % of Ly- $\alpha$  and a mean photon energy of 9.27 eV. The photon flux is  $6.4 \times 10^{13}$  photons  $cm^{-2}s^{-1}$  at sample position.

### 2.1.3 Extreme EUV source

To simulate the solar EUV irradiation reflected by IPM on both Charon and interstellar ices, we use the HF-CGM high – flux beam line of the National Synchrotron Radiation Research Center in Hsinchu, Taiwan. It provides a continuum EUV to VUV photons from 4 to 40 eV. The continuum is separated into monochromatic He II line (30.4nm) with a six-meter cylindrical grating monochrometer with an incident angle of 70 degrees. With the help of a movable entrance slit and movable curved exit slit, the energy resolving power can reach around  $3 \times 10^4$  at 40 eV for grating 1600 l/mm with both slits movable and set opening to



10  $\mu\text{m}$  (Hsieh 1998). Similar to VUV irradiation provided by MDHL, the light intensity was monitored by the same nickel mesh with photoelectric efficiency obtained by SXUV 100 photodiode calibrated by NIST. With the known photoelectric efficiency, the flux of monochromatic 30.4nm is measured to be  $2.15 \times 10^{14} \text{ photons } s^{-1} \text{ cm}^{-2}$  with a spot size of 1 cm

## 2.2 Experimental Protocol

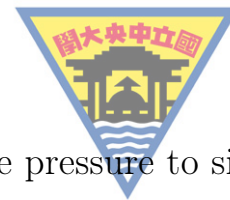
In this section, we will briefly introduce the procedures of how we performed our experiments. It is divided into four parts, preparation and cooling, deposition, irradiation and warmup.

### Preparation of experiments and cooling

Before any of experiment is done, we bake our system at 100 oC for 48 hours to reduce the contamination of water and residue gases as much as possible. It was cooled to room temperature that the background pressure can reach routinely at  $1 \times 10^{-10}$  torr. The gasline were connected with the regulators of the gas tanks and bake to 100 °C and pumped by molecularturbo pump for two days before any experiment were done. Also, The water sample has been freeze thaw several times by liquid nitrogen until there is no pressure increase recorded by baratron when water is freezed. Before cooling the substrate to cryogenic temperature, we took an IR spectrum and started the monitoring of residue gases by QMS in order to compare the residue molecules and to verify any possible contaminations in the main chamber. We then start the cooling process thanks to the closed-cycle He cryostat.

### Deposition

The gas mixtures are pre-mixed in our gasline system introduced in section 2.1.1. We used a leak valve to condense the gas from the stainless steel bottles onto pre-cooled KBr substrate at 14 K, which monitored by Fourier transformed Infra-red spectroscopy (FTIR) and Quadrupole mass spectrometer (QMS) during deposition. The pressure of deposition is fixed to  $1 \times 10^{-8}$  torr that the deposition rate is  $4 \times 10^{16} \text{ molecules cm}^{-2} \text{ min}^{-1}$ . After deposition, we placed the ice mixture at 14 K for 60 minutes and to allow pumping of residue gas, until



pressure of the main chamber reduce back to its base pressure to simulate the interstellar environment before irradiation.

### Photon Irradiation

The total irradiation time is 270 to 450 minutes depend on experiment configurations; with time intervals varies from 2 to 30 minutes. After each irradiation, we waited for 10 minutes allowing pumping out of the photodesorpted gas molecules. During irradiation, the photon flux is monitored by a nickel mesh. After Irradiation, we place the sample for 30 minutes to observe if any thermal reaction was conducted.

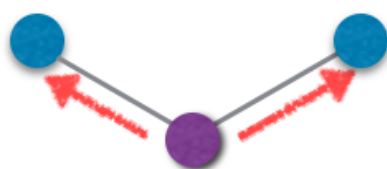
### Warmup

We use 1 K/min to warmup the substrate to 300 K to demonstrate effects of a new born star nearby an interstellar cloud. During warmup, we record the QMS from 1 to 100 a.m.u. to observe if there are low quantity of higher mass product formed during irradiation.

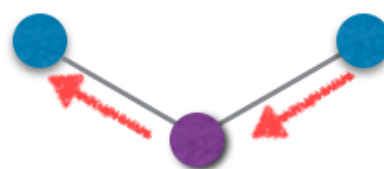
## 2.3 Infra-red spectroscopy and the Beer's Law

We used infra-red spectroscopy extensively in chapter 3 and 4, it is a powerful tool in studying molecular interactions during irradiation and warmup. We choose infra-red rather than Ramen spectroscopy because infra-red has lower energy that it would not change the structure of the ice mixture nor breaking any of the bonds. With different vibration modes, the energy absorbed by molecules are quantized. With the energy of absorption bands in infra-red spectrum, we may identify the functional group of the species. To simply classify, molecules can have, from less energetic, translational, rotational and vibrational motions. Generally, vibrational motions can be divided into stretching and bending. Stretching needs more energy than bending. For stretching, there exist Symmetric and Asymmetric stretching, while bending can be divided into In-plane Scissoring, rocking and out of plane Wagging and Twisting (Figure 2.4).

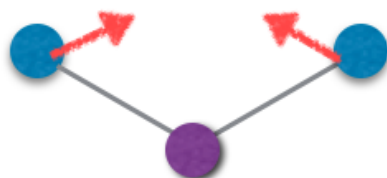
By Beer's Law, we may calculate the column density of the molecule



Symmetric



Asymmetric



In-plane Scissoring



In-plane Rocking



Out of plane Wagging



Out of plane Twisting

- indicate motion out of the page
- indicate motion into the page

Figure 2.4: Different vibrational modes of a three atom molecule.



with its functional groups, which are used to plot figures in chapter 3 and 4. Beer Lambert's Law suggest that when light passes through a medium, amount of light absorbed is proportional to density and path length of the medium. Assume the known intensity beam  $I_0(\nu)$  passes through the medium and beam intensity become  $I(\nu)$ . The transmittance  $T(\nu)$  is defined by equation 2.1.

$$T(\nu) = \frac{I(\nu)}{I_0(\nu)} \quad (2.1)$$

Also, the absorbance  $a(\nu)$  is defined by equation 2.2.

$$a(\nu) = -\ln T(\nu) = -\ln \frac{I(\nu)}{I_0(\nu)} = nl\sigma(\nu) \quad (2.2)$$

where  $n$  is number density (molecules/cm<sup>3</sup>),  $l$  is the path length (cm),  $\sigma(\nu)$  is the cross-section (cm<sup>2</sup>/molecule) of corresponding frequency  $\nu$ . This equation is known as Lambert Beer's Law.

As the ice mixture in our thesis are at 14K, the peaks of absorbance are often a broadband due to coupling between neighbor molecules. Therefore, we can integrate the whole band of the peak equation 2.2 with respect to frequency and use the absorbance strength ( $A$  value) in literatures to calculate the column densities  $N$  of the ices by equation 2.3.

$$N = \frac{\int a(\nu) d\nu}{A(\nu)} \quad (2.3)$$

where  $N$  is the column density (molecule cm<sup>-2</sup>),  $A(\nu)$  is the absorbance strength (cm molecule<sup>-1</sup>).

## 2.4 Reaction Rate Laws

In this section, we will introduce rate reaction of a consecutive reaction and the concept of pseudo first order which we used to fit our reaction product against irradiation time. The rate of a chemical reaction is the relation between change in concentration of a substance per unit of time. i.e. For a balanced chemical reaction,  $A \rightarrow 2B$ , the rate of





reaction is  $-\frac{\Delta[A]}{\Delta t}$ . The formation rate of B is 2 times destruction rate of A.

When there are two reactants, with balanced equation  $2A + B \rightarrow 2C$ . The reaction is a third order overall, second order in A and first order in B. rate  $= k[A]^2[B]$ .

To determine the order of a reaction, we can only determine it experimentally. One way is method of initial rates. By changing concentration of initial reactants, and find out the initial reaction rate, we may find out the relation between two reactants and the rate. i.e. rate  $= k[A]^x[B]^y$ . For a reaction with only one reactant  $[R]$ , we may use the relation between time and reactant concentration to plot graphs to find out the order of reaction. For a zero order reaction, the rate is not depending on any reactant that it is a constant. The rate  $= -\frac{\Delta[R]}{\Delta t} = k[R]^0$ . By calculus,  $[R]_0 - [R]_t = kt$ .

For a first order reaction, rate  $= -\frac{\Delta[R]}{\Delta t} = k[R]$ . By calculus,  $\ln[R]_t = -kt + \ln[R]_0$ .

For a second order reaction, rate  $= -\frac{\Delta[R]}{\Delta t} = k[R]^2$ . By calculus,  $\frac{1}{[R]_t} - \frac{1}{[R]_0} = kt$ .

Hence, if we get a straight line in a plot between time as x-axis, and the concentration of reactant as y axis, it is a zeroth order reaction, similarly, in first order reactions, we get straight line in plots between  $\ln[R]$  as y axis and t in x axis.

In a reaction with one reactant in excess, the rate of reaction is called pseudo first order reaction where pseudo means pretended. For  $A+B \rightarrow C$ , rate  $= k[A][B]$ . As  $[B]_0 \gg [A]_0$ , change of  $[B]$  is negligible that  $[B] \sim [B]_0$ . Therefore,  $[B]$  is assumed to be a constant and included in the rate constant k.

For a consecutive reaction, where  $A \rightarrow B \rightarrow C$  that the produced product will not convert back as reactant. A simple example is radioactive decay. At  $t = 0$ ,  $[A] = [A]_0$ ,  $[B] = 0$ ,  $[C] = 0$  and at all times,  $[A] + [B] + [C] = [A]_0$ . The rate equations are as follows:

$$-\frac{\Delta[A]}{\Delta t} = k_1[A] \quad (2.4)$$





$$-\frac{\Delta[B]}{\Delta t} = k_1[A] - k_2[B] \quad (2.5)$$

$$-\frac{\Delta[C]}{\Delta t} = k_2[B] \quad (2.6)$$

By equation 2.4, we get

$$[A] = [A]_0 e^{-k_1 t} \quad (2.7)$$

By substituting equation 2.7 into equation 2.5, we get

$$-\frac{\Delta[B]}{\Delta t} + k_2[B] = k_1[A]_0 e^{-k_1 t} \quad (2.8)$$

After solving the differential equation 2.8, we get

$$[B] = \frac{k_1}{k_2 - k_1} (e^{-k_1 t} - e^{-k_2 t}) [A]_0 \quad (2.9)$$

Finally, since  $[C] = [A]_0 - [B] - [A]$ , by equation 2.7 and 2.9, we get

$$[C] = \left( 1 + \frac{k_1 e^{-k_2 t} - k_2 e^{-k_1 t}}{k_2 - k_1} \right) [A]_0 \quad (2.10)$$

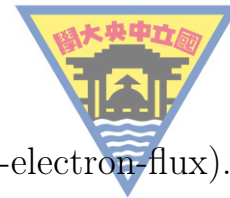




### 3. Experimental Results of $\text{CH}_4 + \text{NH}_3$ ice mixtures

According to Grundy et al. (2016),  $\text{CH}_4$  from Pluto may accumulate by cold-trapping, onto surface of Charon. The amount of  $\text{CH}_4$  varies throughout the surface of Charon because it depends on duration of temperature below 25 K. The duration depends on diurnal motion and thermal inertia of Charon. With a tilted axis of 112 degrees to the ecliptic, higher concentration of  $\text{CH}_4$  will accumulate at the pole (see chapter 1 for details). Therefore, we investigate different concentrations of  $\text{CH}_4 + \text{NH}_3$  ice mixtures and answer several questions: Will different concentration of  $\text{CH}_4$  mix with high concentration of ammonia observed on crater position and throughout the surface of Charon (Grundy et al. 2016) have structure difference in accumulation of tholin? Are there variations of photo-products when concentration of  $\text{CH}_4$  differ during warm-up? Since both EUV and VUV irradiation irradiates onto Charon, are there any differences when we change the photon source from VUV to EUV to irradiate the ice mixtures?

The main source to irradiate the dark side of Charon is  $\text{Ly } \alpha$  reflected by interplanetary medium (Grundy 2016). Other sources such as the energetic ions in solar wind, consists of mainly  $\text{H}^+$ ,  $\text{He}^+$ ,  $\text{He}^{++}$  and  $\text{O}^{2+}$  etc are originated from solar corona or IPM. These ions would also reflect solar irradiation to the dark side of Charon. Among these irradiations, we picked He II irradiation because He II is 3 – 20 times more intense than He I during a solar flare. As it varies, it is difficult to estimate the dose onto Charon. Besides, electronic flux is also present in solar wind but it is one order of magnitude lower than proton flux. The flux for energetic electrons observed at the 1 A. U. position is



available (<http://www.swpc.noaa.gov/products/goes-electron-flux>). Although electron flux is much less important than  $\text{Ly } \alpha$ , and their flux varies, we also compare the electron irradiation experiment done by Kim and Kaiser (2011) on  $\text{CH}_4 + \text{NH}_3$  ice mixtures in this chapter.

When Charon is shine by direct sun light, the surface temperature increases and deliver the heat to the poles by conduction. From the model of Grundy et al. (2016), the surface temperature of the pole area would increase to 60 K that the heating rate depends on the thermal conductivity of Charon. To demonstrate the heating process, we warmup our ice mixture with a heating rate 1 K/min and monitor the ice by both QMS and scanning IR spectra with 5 K intervals. We will look into whether there are new species formed during warmup and monitor the gas phase desorption.

Finally, in this chapter, after we focus on the concentration effect of  $\text{CH}_4$  on photo-products, photon energy effects, species detected during warmup phases, we present the residues accumulated by irradiating  $\text{CH}_4 + \text{NH}_3$  ice mixtures with different ratios. Since both tholin formed on Titan and Charon has similar colour, we also compare the IR spectra of MDHL, NSRRC with different configurations with the residues on Titan with experiments done by Imanaka et al.

### 3.1 3.1.1 The concentration effect of $\text{CH}_4$ on production of $\text{C}_2\text{H}_6$ and $\text{CN}^-$

We first look into the concentration effects of  $\text{CH}_4$  by irradiation by VUV irradiation. Before and after deposition, we scanned an IR spectrum and plotted the absorbance of the ice mixtures. figure 3.1.1 plots the absorbance of the  $\text{CH}_4 + \text{NH}_3$  ice mixtures in different ratios. Due to the ice thickness, the infra-red spectrum of  $\text{CH}_4 + \text{NH}_3 = 3:2$  consist of 900 ML of  $\text{CH}_4$  and 600 ML of  $\text{NH}_3$  is tilted due to interference. Since the amount of ammonia is fixed (600 ML) in all the ratios, other ratios has less  $\text{CH}_4$  and this problem is less serious. This is also not



observed in the ice mixtures after irradiation. Using the same reference spectrum, that is the infra-red spectrum recorded before deposition, we plotted the infra-red spectrum of irradiated ice mixture in figure 3.1.2. It shows the absorbance of each ratio after irradiation. We labelled the peaks which we used to calculate the column densities onto the graph. Main products we have detected are  $\text{C}_2\text{H}_6$ ,  $\text{CN}^-$  and  $\text{C}_3\text{H}_8$ . The peak positions with the references are listed at 3.1.

Table 3.1: The peak positions of identified substances after irradiation in different configurations of ice mixtures.

Literture assignments		$\text{CH}_4 + \text{NH}_3$ ratio (MDHL)				Ref.
Wavenumber ( $\text{cm}^{-1}$ )	Carrier	1:5 ( $\text{cm}^{-1}$ )	1:10 ( $\text{cm}^{-1}$ )	1:20 ( $\text{cm}^{-1}$ )	3:2 ( $\text{cm}^{-1}$ )	
3375	$\nu_3$ ( $\text{NH}_3$ )	3366	3366	3369	3367	1
3290	$2\nu_4$ ( $\text{NH}_3$ )	-	-	-	-	1
3210	$\nu_1$ ( $\text{NH}_3$ )	3207	3208	3210	3205	1
3011	$\nu_3$ ( $\text{CH}_4$ )	-	-	-	-	2
2972	$\nu_{10}$ ( $\text{C}_2\text{H}_6$ )	2975	-	-	2975	3
2960	$\text{C}_3\text{H}_8$	-	-	-	2960	7
2941	$\nu_8 + \nu_{11}$ ( $\text{C}_2\text{H}_6$ )	2940	-	-	2940	3
2904	$\nu_1$ ( $\text{CH}_4$ )	2901	-	-	2901	5
2879	$\nu_5$ ( $\text{C}_2\text{H}_6$ )	2882	2883	-	2882	3
2814	$\nu_2 + \nu_4$ ( $\text{CH}_4$ )	-	-	-	2815	5
2083	$\nu$ ( $\text{CN}^-$ )	2088	2087	2088	2088	2
1625	$\nu_4$ ( $\text{NH}_3$ )	1625	1625	1626	1631	1
1514	$\delta$ ( $\text{NH}_2$ )	1509	1507	1505	1511	6
1465-1440	deform $\text{CH}_2$ scissor	1461	-	-	1463	3,4
1390-1370	$\text{CH}_3$ sym deform	1394	1394	1394	1372	4
1298	$\nu_4$ ( $\text{CH}_4$ )	1301	1302	1305	1299	2
1075	$\nu_2$ ( $\text{NH}_3$ )	1073	1072	1072	1072	1
820	$\nu_{12}$ ( $\text{C}_2\text{H}_6$ )	-	-	-	820	3

Reference: 1. Bossa et al 2008 2. Moore and Hudson 2003 3. Kim et al. 2010 4. Socrates 2001 5. Bennet and Kaiser 2007 6. Zheng et al. 2008 7. Hudson and Moore 2004

From infra-red absorption spectrum and their positions, we assigned the peak  $2086 \text{ cm}^{-1}$  to  $\text{CN}^-$  but not a combination of HCN and  $\text{CN}^-$  because of we cannot observe the HCN bending mode located at  $848 \text{ cm}^{-1}$ . Although in the case  $\text{CH}_4 + \text{NH}_3 = 3:2$ , we may observe a peak located at  $820 \text{ cm}^{-1}$ , the peak is with a FWHM half of HCN and it disappeared at 50 K. Since 50 K is the desorbing temperature of  $\text{C}_2\text{H}_6$  and the position is  $\nu_{12}$  mode of  $\text{C}_2\text{H}_6$ , we assign the  $820 \text{ cm}^{-1}$  peak as  $\text{C}_2\text{H}_6$ . As the absence of HCN bending mode, we may assign our peak located at  $2086 \text{ cm}^{-1}$  as  $\text{CN}^-$ . Other assignments such as  $\text{C}_2\text{H}_6$  and  $\text{C}_3\text{H}_8$  are observed with multiple peaks.



We integrated the area and divided by the absorption strength stated in table 3.2. Although we understand that there is an average error in absorption strengths of no more than 10 % when the pure ice is diluted in  $N_2$  and  $H_2O$  (Richey and Gerakines 2012). In our case, absorption strengths changes after  $CH_4$  and  $NH_3$  are mixed. For example, according to d' Hendecourt and Allamandola (1986), the band of  $NH_3$  located at  $1070\text{ cm}^{-1}$  would not change much (from  $1.1 \times 10^{-17}$  to  $1.2 \times 10^{-17}$ ) when excess water is added to pure  $NH_3$  and therefore, we may use the same absorption strength throughout our discussion to give a brief concept on what is the column density of the species and how is the absorption area changes when concentrations of ice mixtures and photon energy are changed. For the case of  $CN^-$ , we know that  $CN^-$  has a bond order =3 by its molecular orbitals which is different from  $CN$  stretching (bond order 2.5) which is very sensitive to the matrix environment. As an example, by Borget et al. (2012), the  $CN$  stretch in amino acetonitrile change by factor of 2 between the pure molecule itself and in a mixture of amino acetonitrile and  $H_2O$  (1:3). Here, we adopt the absorption strengths stated in Table 3.2 and neglect the error in absorption strengths.

Table 3.2: The strength of absorbance adopted in this thesis measured in literatures of pure ice samples

Wavenumber ( $\text{cm}^{-1}$ )	Assignment	Vibration	FWHM	A value ( $\times 10^{-17}$ )	Reference
2976	$C_2H_6$	$-CH_3$	-	1.05	2
2960	$C_3H_8$	$-CH_2-$	-	2.58	2
2086	$CN^-$	$CN$	-	1.8	3
1297	$CH_4$	$CH$ deformation	8	0.61	1
1070	$NH_3$	"umbrella mode"	68	1.7	1

Reference: 1. d'Hendecourt and Allamandola (1986) 2. Moore and Hudson (1998) 3. noble et al. (2013)

## 3.2 3.1.1 Reaction mechanisms

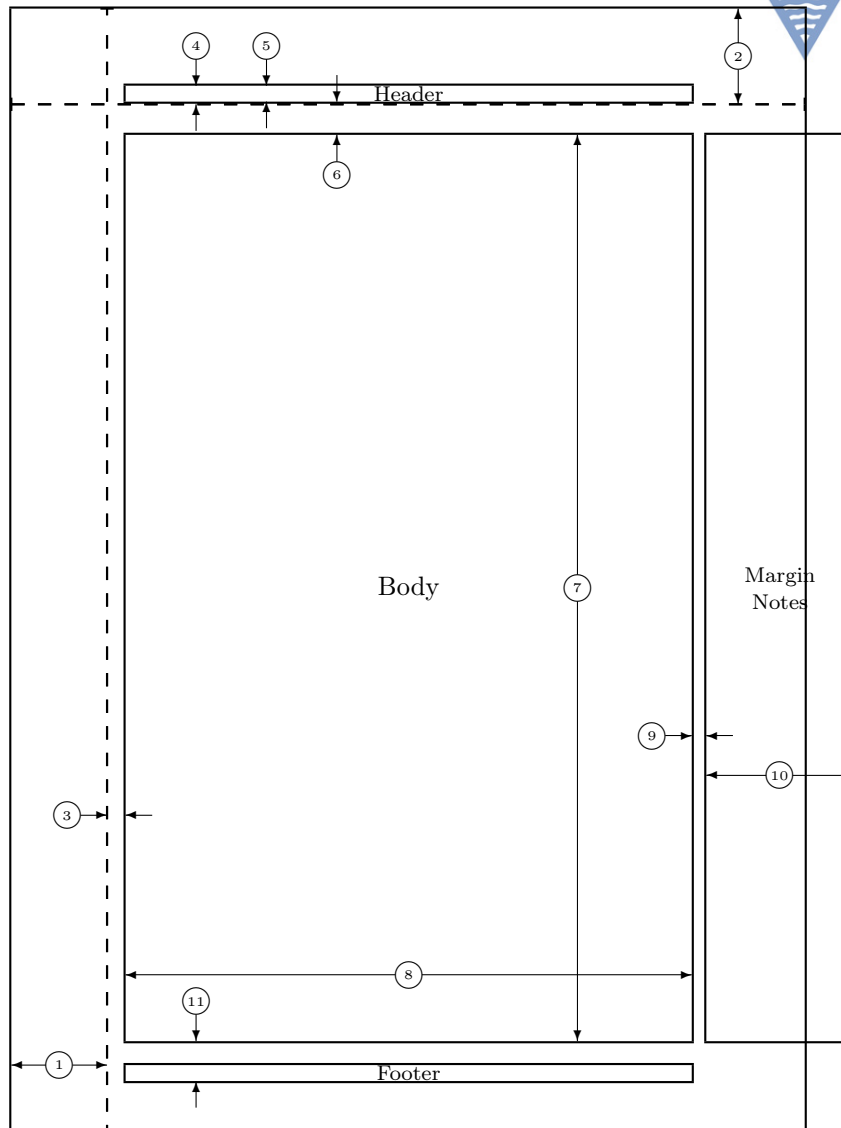
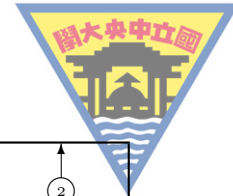


## Bibliography

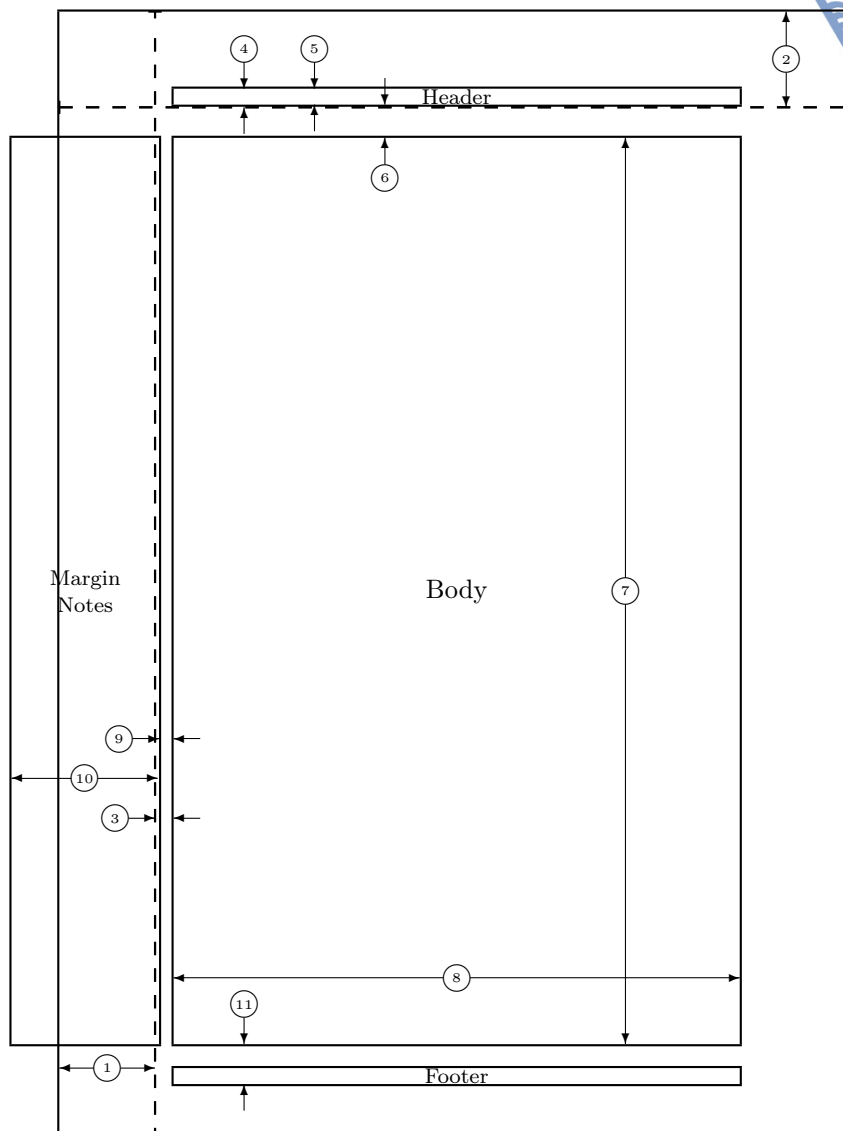
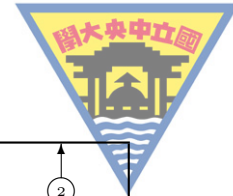
- [1] Donald E. Knuth. *The TEXbook, Volume A of Computers and Typesetting*. Addison-Wesley, Reading, Massachusetts, second edition, 1984, ISBN 0-201-13448-9.  
<http://www-cs-staff.stanford.edu/~knuth/index.html>
- [2] Leslie Lamport. *LaTeX: A Document Preparation System*. Addison-Wesley, Reading, Massachusetts, second edition, 1994, ISBN 0-201-52983-1.
- [3] J. LO, *eThinking in Circuits with PSpice*. Cavesbooks, Inc., 2012, ISBN 978-957-41-8721-8.
- [4] —, *aThinking in Control with Matlab*. Cavesbooks, Inc., 2012, ISBN pending.
- [5] —, *LaTeX & U 自助出版*. 中央敦煌, 北科文具部, 2012, ISBN 978-957-41-9448-3.
- [6] —, *Packages author of ncuthesis(CJK, Xe), bizcard, cnwritingCJK*. Free packages, 2012.  
<https://code.google.com/p/ncu-thesis-latex-template/>
- [7] *Writing a thesis in LaTeX* <http://texblog.org/>
- [8] Chinese character \CJK within \section{} does not work using pdfLaTeX, + \includegraphics,  
<http://tex.stackexchange.com/a/126570>
- [9] *Page numbers only appear on pages where a chapter starts*,  
<http://tex.stackexchange.com/a/79776>







1	one inch + \hoffset	2	one inch + \voffset
3	\oddsidemargin = 14pt	4	\topmargin = -14pt
5	\headheight = 12pt	6	\headsep = 25pt
7	\textheight = 682pt	8	\textwidth = 426pt
9	\marginparsep = 11pt	10	\marginparwidth = 111pt
11	\footskip = 30pt		\marginparpush = 5pt (not shown)
	\hoffset = 0pt		\voffset = 0pt
	\paperwidth = 597pt		\paperheight = 845pt



1	$\text{one inch} + \backslash\text{hoffset}$	2	$\text{one inch} + \backslash\text{voffset}$
3	$\backslash\text{evensidemargin} = 14\text{pt}$	4	$\backslash\text{topmargin} = -14\text{pt}$
5	$\backslash\text{headheight} = 12\text{pt}$	6	$\backslash\text{headsep} = 25\text{pt}$
7	$\backslash\text{textheight} = 682\text{pt}$	8	$\backslash\text{textwidth} = 426\text{pt}$
9	$\backslash\text{marginparsep} = 11\text{pt}$	10	$\backslash\text{marginparwidth} = 111\text{pt}$
11	$\backslash\text{footskip} = 30\text{pt}$		$\backslash\text{marginparpush} = 5\text{pt}$ (not shown)
	$\backslash\text{hoffset} = 0\text{pt}$		$\backslash\text{voffset} = 0\text{pt}$
	$\backslash\text{paperwidth} = 597\text{pt}$		$\backslash\text{paperheight} = 845\text{pt}$